A&A 524, A73 (2010)
DOI: 10.1051/0004-6361/201015178

Astronomy & Astrophysics

Multi-instrument measurement campaign at Paranal in 2007

Characterization of the outer scale and the seeing of the surface layer

W. Dali Ali[1], A. Ziad[1], A. Berdja[1,4], J. Maire[1,5], J. Borgnino[1] M. Sarazin[2], G. Lombardi[2], J. Navarrete[2], H. Vazquez Ramio[3], M. Reyes[3], J. M. Delgado[3], J. J. Fuensalida[3], A. Tokovinin[4], and E. Bustos[4]

[1] OCA. CNRS UMR 6525 Hippolyte FIZEAU, Université de Nice-Sophia Antipolis, Campus Valrose, 06108 Nice Cedex 2, France
e-mail: daliali@unice.fr
[2] European Southern Observatory, Karl-Schwarzschild-Str.2, 85748 Garching, Germany
[3] Instituto de Astrofísica de Canarias via Lactea s/n, 38200 La Laguna, Tenerife, Spain
[4] Cerro Tololo Inter-American Observatory, Casilla 603 La Serena, Chile
[5] Département de Physique, Université de Montréal, C.P. 6128, Succ. Centre-Ville, Montreal, QC, H3C 3J7, Canada

Received 8 June 2010 / Accepted 5 September 2010

ABSTRACT

Aims. Within the framework of site qualification for the future European large telescope E-ELT, a campaign of measurements was carried out for ten nights in December 2007 at Paranal using six independent instruments.
Methods. To characterize the optical turbulence, two techniques were used: the statistical analysis of the fluctuations of the angle of arrival and the scintillation of the observed objects which are, in this case, a single star for DIMM, GSM, and MASS, a double star for Cute-SCIDAR, and Moon limb for MOSP and LuSci.
Results. The optical parameters measured in this campaign and presented here are the seeing, the isoplanatic angle, the coherence time, and the outer scale. We obtain a good agreement with the value measured in previous campaigns. We also extracted the vertical profile of the turbulence given by $C_n^2(h)$, and the profiles of the outer scale for the first time at Paranal. A comparison of the different results that we present here allows the determination of the energy distribution in the free atmosphere, on the ground layer as well as in the first meters above ground. This reveals a significant contribution of the surface layer to the degradation of the global seeing.

Key words. instrumentation: detectors – atmospheric effects – site testing – methods: data analysis – techniques: high angular resolution

1. Introduction

The atmospheric turbulence induces a random distortion of the wavefront, which limits the performance of the high angular resolution observations. Adaptive Optics (AO) and fringe tracking (FT) systems were developed to compensate the optical effects of the atmosphere. These techniques need however a quantitative spatiotemporal and angular characterization of the wavefront. Thus, in addition to the measurement of the seeing, which is responsible for the image spread, it is necessary to characterize the variation of the wavefront behavior in the decametric range. This is crucial for the new generation of large telescopes such as the European Extremely Large Telescope and the Thirty-Meter Telescope.

Classical parameters that describe the optical turbulence energy are the seeing ε_0 or Fried parameter r_0. The seeing is measured in most observatories by means of differential image motion monitors (DIMM). The isoplanatic angle θ_0 determines the angular coherence field of view. The coherence time τ_0 is the characteristic time of the turbulence evolution that is relevant to AO and FT systems. Finally, the outer scale of the spatial coherence of the wavefront $\mathcal{L}_0$ becomes of importance for the telescopes of growing apertures and for long baseline interferometers.

In this paper we present the results of the Paranal campaign conducted by three teams working in collaboration (Dali-Ali et al. 2009). The advantage of this campaign is the use of several instruments to measure simultaneously the optical parameters and the turbulence profiles. This allowed us to collect quantitative data, including the extraction of the first profiles $\mathcal{L}_0(h)$ for the Paranal site, and gave the possibility to separate the contributions of free atmosphere, ground layer, and surface layer from the whole turbulence effect.

In Sect. 2, we give the description of the different instruments used during this campaign. Their localization and the conditions of observation for ten nights is given in Sect. 3. In Sect. 4, we present the results of measurements of each parameter night by night, followed by a mean value for the whole campaign. A comparison of the results is given in Sects. 5 and 6, where we separate the surface layer contribution from the whole atmosphere.

2. Instruments of the Paranal site-testing campaign

Two important aspects were considered in this campaign, the first one is the value of each parameter integrated at the ground level; this determines the global turbulence characteristics of the Paranal site. The second one is the vertical distribution of this turbulence from the ground to the top of the atmosphere.

2.1. Integrated turbulence monitors

2.1.1. The ESO-DIMM (differential image motion monitor)

The ESO-DIMM is placed on a tower at 6m above the ground. It was the main element of the instrumentation developed for the VLT site evaluation campaign (Sarazin 1986). It works in robotic

mode at Paranal since 1998. It is a 35 cm telescope masked with two 11 cm circular sub-apertures. A thin-wedge prism is placed at one aperture to separate the two images of the observed star in the focal plane. A CCD detector takes series of images with 5 ms exposure time. The measurement of the differential image motion will separate the effect of atmospheric turbulence from the telescope vibrations. Using the Kolmogorov model, the seeing defined as the full width at half maximum (FWHM) of the point spread function (PSF) is related to the variance of the differential image motion (Sarazin & Roddier 1990). The coherence time and isoplanatic angle are estimated by the method of Sarazin & Tokovinin (2002).

2.1.2. The GSM (generalized seeing monitor)

The GSM is dedicated to the measurement of optical parameters that are deduced from angle of arrival (AA) spatio-temporal statistics. Parameters of interest are seeing, outer scale of turbulence, isoplanatic angle, and coherence time for AA fluctuations τ_{AA}. The experiment consists of independent synchronized 10 cm telescopes modules measuring the AA fluctuations at different points of the wavefront. The modules are mounted in a non-redundant configuration. This allows the determination of the outer scale parameter from the AA covariance. Usually GSM is composed of four separate modules with six baselines. Six modules were used for a better sampling of the AA covariance with 15 baselines exclusively for this campaign. This also enabled us to validate the atmospheric model (Maire et al. 2008). Two modules were placed on the same mount to measure the seeing with the DIMM method (see Ziad et al. 2004).

2.2. Turbulence profilers

2.2.1. The Cute-SCIDAR (scintillation detection and ranging)

An upgraded version of a generalized SCIDAR has been used. It has been developed for Paranal by the IAC (Vazquez Ramio et al. 2008). New features during this campaign were the real-time measurement of turbulence profiles and the remote control of the instrument. It was mounted on the VLTI Auxiliary Telescope 4 (AT4). Cute-SCIDAR provides the vertical profile of the turbulence energy $C_n^2(h)$ by measuring the scintillation of double stars with a CCD. It is deduced from the spatial auto-correlation functions of the scintillation in two directions, parallel and perpendicular to the double stars separation (Avila et al. 1997). The vertical resolution depends on the double star angular separation; for the Cute-SCIDAR it was about 300 m. The integrated optical parameters, seeing and isoplanatic angle, are deduced from the profiles.

2.2.2. The MASS (multi aperture scintillation sensor)

In MASS, the light of a single star is received by a system of four concentric apertures, with 2 cm inner aperture and 13 cm for the outer one. The beam splitting between annular apertures is done by internal optics (Kornilov et al. 2003). Scintillation, which depends on the altitude of the turbulence, is detected in each aperture using photomultipliers with 1 ms exposure time. The apertures and their combinations act as spatial filters, separating the contributions from different altitudes. The MASS measures a coarse turbulence profile $C_n^2(h)$, the coherence time and the isoplanatic angle. However, MASS does not sense the near-ground turbulence and does not work under strong scintillation (Tokovinin & Kornilov 2007).

2.2.3. The LuSci (lunar scintillometer)

The LuSci is used to probe the turbulence in the ground and surface layer. Its principle is the measurement of Moon scintillation. Over a set of detectors at fixed separations (baselines), a normalized scintillation covariance is measured. Each covariance is related to $C_n^2(h)$ with its proper weighting function, which depends on detector configuration (size, baseline separation and orientation) as well as on the lunar phase (Rajagopal et al. 2008; Tokovinin 2007; Tokovinin et al. 2010). In this campaign, LuSci had four detectors spaced linearly from 2 cm to 38 cm. A smooth profile is fitted to the measured covariances. Turbulence integrals to the heights from 6 m to 256 m are calculated from the fitted profiles. During the campaign, the instrument was almost totally automated.

2.2.4. The MOSP (monitor of outer scale profile)

The MOSP is the only instrument able to extract the outer scale profiles. It is a 29-cm telescope with a impressive focal length (10 m). The principle of the instrument is based on the measurement of AA fluctuations by observation of the moon limb. The spatioangular correlations of the AA in different angular separations depends on the vertical profiles of the turbulent energy $C_n^2(h)$ and on the vertical profiles of outer scale $\mathcal{L}_0(h)$. Determining both profiles by inversion leads to unstable results. Instead, we used the $C_n^2(h)$ simultaneously measured by the Cute-SCIDAR and determined only $\mathcal{L}_0(h)$ by the simulated annealing algorithm. MOSP is equipped with a PixelFly CCD and a Barlow lens to extend the focal length. This increases the sensitivity of the monitor to the fluctuations of the moon limb. The exposure time was set to 1 or 2 ms in order to freeze the atmospheric effects on image motion (Maire et al. 2007).

3. Campaign setup

The instruments GSM, MOSP, MASS, and LuSci were installed at a height of 1.5 m from the ground. They were located near the ESO-DIMM tower of 6 m height at the northern side of the VLT platform. The Cute-SCIDAR was mounted some distance a part in the AT dome of 5 m height, as shown in Fig. 1.

The observations started on 2007 December 17, and continued for ten nights until December 26. Most instruments were simultaneously in operation. This allowed us to collect a substantial database for cross-comparisons of the results produced by each instrument. A common list of targets was provided for the instruments observing single stars.

We collected data from the meteorological station located near the ESO-DIMM (Fig. 1). The sampling intervals were 2 s for digital sensors (wind speed and direction) and one minute for analogic sensors measuring temperature, relative humidity, and pressure (T, Rh, P).

4. Integrated characteristics of atmospheric turbulence

4.1. Seeing

The relation between seeing ε_0, Fried parameter r_0, and the turbulence integral is given by Roddier (1981),

$$\varepsilon_0 = 0.98\lambda/r_0, \quad (1)$$

$$r_0^{-5/3} = 16.7\lambda^{-2}(\cos\gamma)^{-1}\int_0^\infty C_n^2(h)\mathrm{d}h, \quad (2)$$

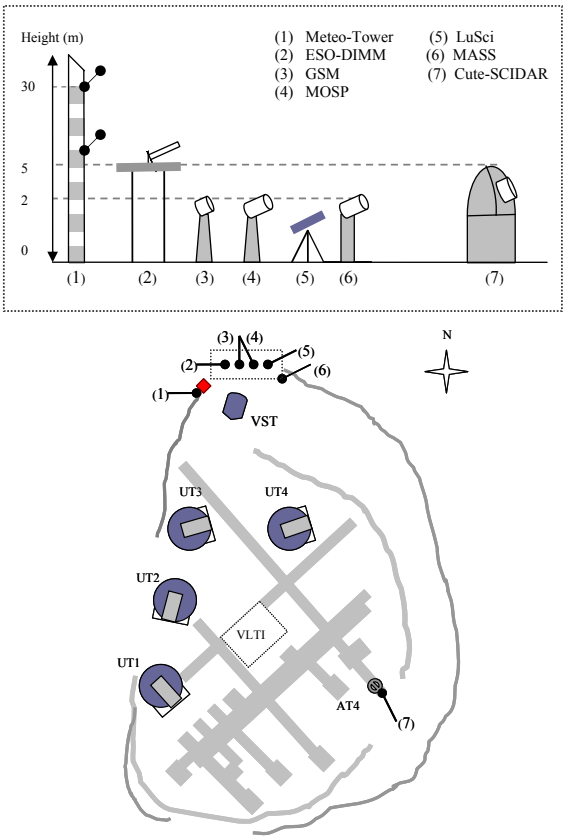

Fig. 1. Setup of turbulence monitors at the Paranal site. GSM, MOSP, LuSci and MASS-DIMM were located at the northern side of the platform near the ESO-DIMM tower. The Cute-SCIDAR was located in the south-eastern side of the platform at the AT4 station.

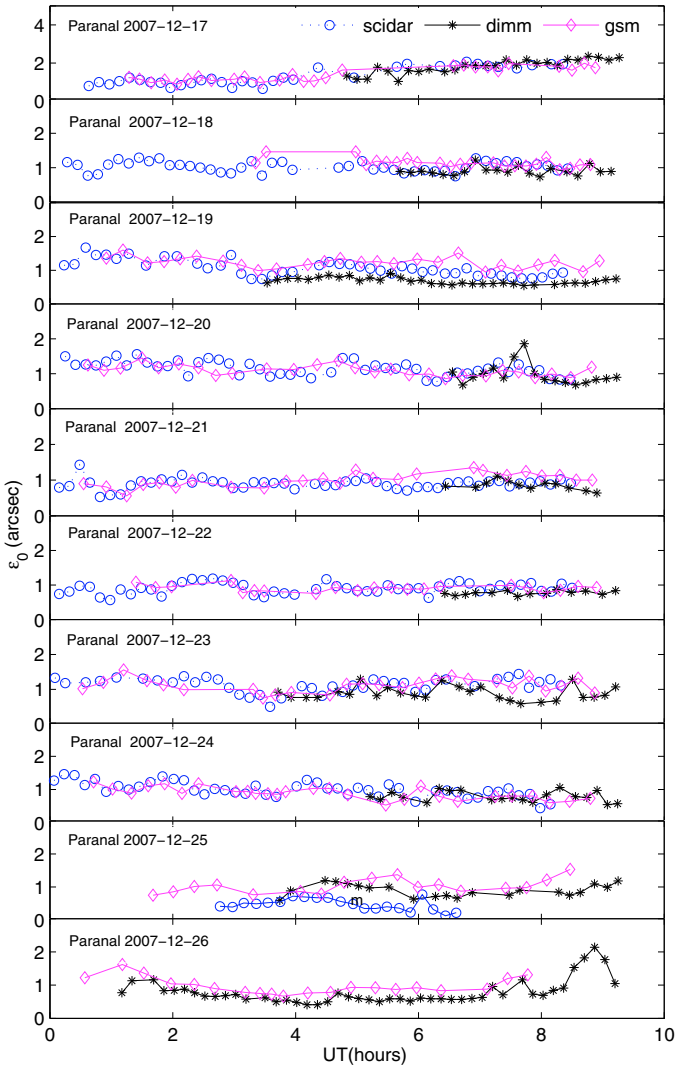

Fig. 2. Seeing measured with ESO-DIMM (asterisks), GSM (diamonds) and Cute-SCIDAR (circles) for ten nights at Paranal, with 10 mn time sampling for all instruments.

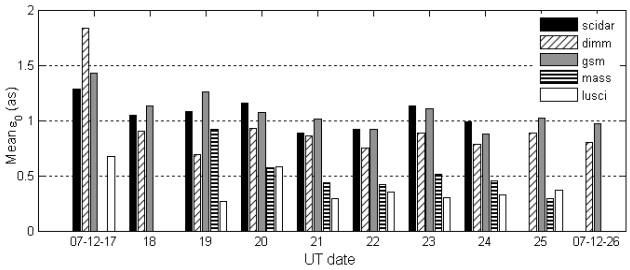

Fig. 3. Mean value of seeing computed on all data delivered by Cute-SCIDAR, ESO-DIMM, GSM, MASS, and LuSci for ten nights at Paranal.

where λ is the wavelength, $C_n^2(h)$ is the optical turbulence energy profile and γ is the zenith angle of the observed object. Below, all atmospheric parameters are given for $\lambda = 500$ nm at zenith. As we note from Eqs. (1) and (2), the contributions of the different layers to the seeing must be summed as 5/3 power ($\epsilon_0^{5/3} = \sum^j(\epsilon_j^{5/3})$), where ϵ_j is the seeing corresponding to the layer at the altitude h_j.

We present in this section the nightly seeing values corresponding to the total turbulence (TOT) measured simultaneously by Cute-SCIDAR, GSM, and ESO-DIMM (Fig. 2). We plot the seeing (and all other parameters) with a 10-min binning. In Fig. 3, we show the mean value of the seeing averaged on all data measured with each instrument for the ten nights. The mean values of the seeing and other parameters are calculated for each instrument using all its data, so the time periods sampled by various instruments during this campaign are slightly different. This can bias the mean values as we can note by comparing Fig. 2 with 3 (e.g. the first night) where the DIMM agrees well with other instruments, but started measuring late.

Figure 2 shows that most of the time, the global seeing values measured by GSM and Cute-SCIDAR agree well but the values given by ESO-DIMM are slightly lower. In Fig. 3 we show the mean value of seeing introduced by the free atmosphere ($h \geq 500$ m) and measured by MASS; it is always less than the global seeing. We also note that the seeing produced by the first 256 m above ground, as measured with LuSci, is comparable to the FA turbulence, especially on the night of December 20. Comparing the thickness of the free atmosphere (FA) (≃15 km) with the layer of 0−255 m, we note that much of the turbulence is concentrated in the first few hundred meters. This point will be further discussed in Sects. 5 and 6.

The mean value of the total seeing during this campaign is 1.07″ for GSM and Cute-SCIDAR and 0.93″ for the ESO-DIMM. It is slightly worse than 0.88″ measured in the previous campaign at Paranal in 1998 (Martin et al. 2000). That last campaign was carried out at about the same time of the year.

4.2. Isoplanatic angle

Fried (1976) defined the AO isoplanatic angle θ_0 as

$$\theta_0^{-5/3} = 2.91 \left(\frac{2\pi}{\lambda}\right)^2 (\cos\gamma)^{-8/3} \int_0^{h_{\max}} C_n^2(h) h^{5/3} \mathrm{d}h. \quad (3)$$

We note that θ_0 depends only on the C_n^2 profile. On the other hand, it was established that the scintillation index σ_I^2 (the normalized intensity variance) is also related to the C_n^2 profile (Roddier 1982)

$$\sigma_I^2 = \int_0^{h_{\max}} W(h) C_n^2(h) \mathrm{d}h, \quad (4)$$

where $W(h)$ is a weighting function that depends on the wavelength λ, the aperture characteristics, and the turbulence spectrum. For $\lambda = 0.5$ μm, $D \simeq 10$ cm and $h \simeq 10$ km, $W(h)$ resembles the $h^{5/3}$ dependence. Then θ_0 can be derived from the scintillation index as (Ziad et al. 2000)

$$\theta_0^{-5/3} = K\sigma_I^2, \quad (5)$$

where K is a constant depending on λ and the aperture characteristics.

For the profilers such as Cute-SCIDAR and MASS, θ_0 is calculated using the measured $C_n^2(h)$ (Eq. (3)), whereas for the ESO-DIMM and GSM it was deduced from the scintillation index (Eq. (5)), taking for each instrument the adequate weighting function. Measurement of θ_0 from the scintillation index is often biased by the finite exposure time. This bias is removed in the data processing for both ESO-DIMM and GSM.

Nightly measurements of isoplanatic angle are plotted in Fig. 4. Obviously, the values given by the ESO-DIMM, GSM and MASS are agree well with those of Cute-SCIDAR for all nights. The mean value of 2.4″ found here (Fig. 5) is close to the 2.6″ measured with the ESO-DIMM in the campaign of 2000 (Sarazin & Tokovinin 2002), whereas in 1998, 1.9″ was found by Martin et al. (2000).

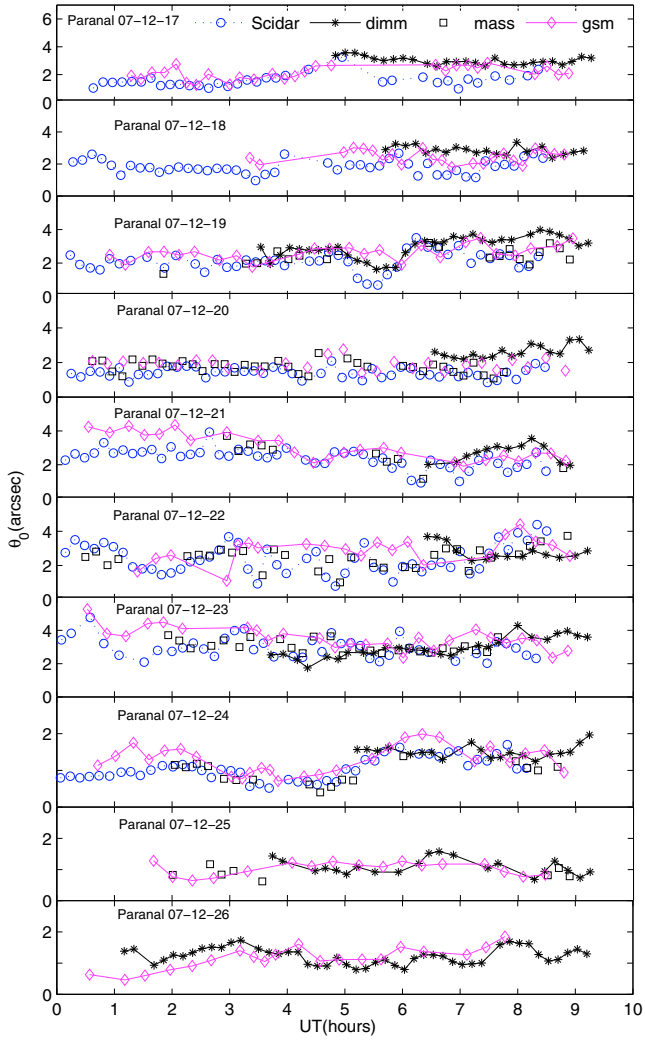

Fig. 4. Isoplanatic angle measured with Cute-SCIDAR (circles), ESO-DIMM (asterisks), GSM (diamonds) and MASS (squares) for ten nights at Paranal with 10 mn time sampling for all instruments.

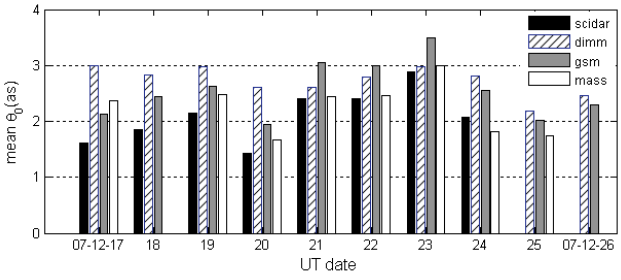

Fig. 5. Mean value of isoplanatic angle computed on all data delivered by ESO-DIMM, GSM, Cute-SCIDAR and MASS for ten nights at Paranal.

4.3. Coherence time

Atmospheric coherence time τ_0 is another important parameter measured in this campaign. The AO coherence time τ_0 (Roddier 1981) is related to the Fried parameter r_0 and the average velocity of the turbulence V_0 as

$$\tau_0 = 0.314 \frac{r_0}{V_0}. \quad (6)$$

For the ESO-DIMM, the coherence time τ_0 can be estimated from the seeing and the instantaneous values of the wind velocity. The wind speed at the 200 mb level $V_{200\ \mathrm{mb}}$ is retrieved from the european center for medium range weather forecasts (ECMWF) data products refreshed every 6 h. We substituted in Eq. (6) the maximum velocity $V_0 = \mathrm{Max}(V_{30\ \mathrm{m}}, 0.4\ V_{200\ \mathrm{mb}})$ following Sarazin & Tokovinin (2002).

For MASS, the τ_0 measurement is based on the temporal analysis of the scintillation signal in the smallest aperture. It does not include the ground layer (GL) turbulence. The coherence time is then corrected for the GL contribution by using the data of the DIMM associated to the MASS as $\tau_0^{-5/3} = (\tau_0^{\mathrm{GL}})^{-5/3} + (\tau_0^{\mathrm{MASS}})^{-5/3}$ with

$$\tau_0^{\mathrm{GL}} = \frac{0.314 r_0^{\mathrm{GL}}}{V_{30\ \mathrm{m}}} \quad (7)$$

and

$$(r_0^{\mathrm{GL}})^{-5/3} = (r_0^{\mathrm{DIMM}})^{-5/3} - (r_0^{\mathrm{MASS}})^{-5/3}. \quad (8)$$

For GSM, the method used to estimate a characteristic time, denoted here as τ_{AA}, consists of processing the structure function of the temporal fluctuations of AA $D_\alpha(r, \tau)$, where α indicates the AA measured with GSM with time difference τ. This temporal structure function saturates for high values of τ, and the point

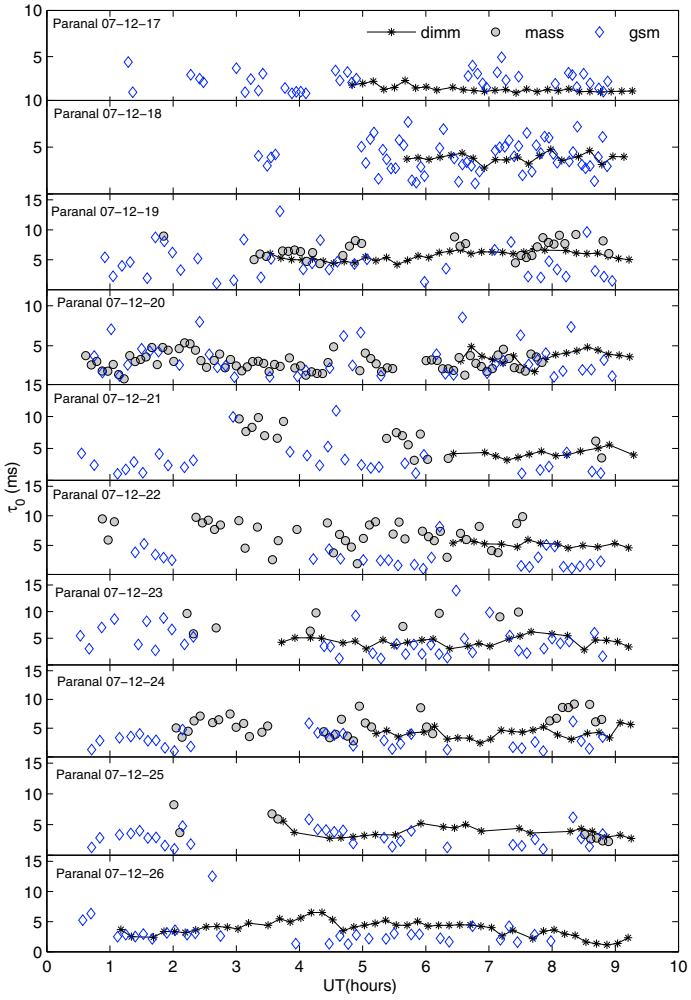

Fig. 6. Coherence time measured with ESO-DIMM (asterisks), GSM (diamonds), and MASS-DIMM (circles) for ten nights at Paranal with 10 mn time sampling for ESO-DIMM and 5 mn for GSM and MASS-DIMM.

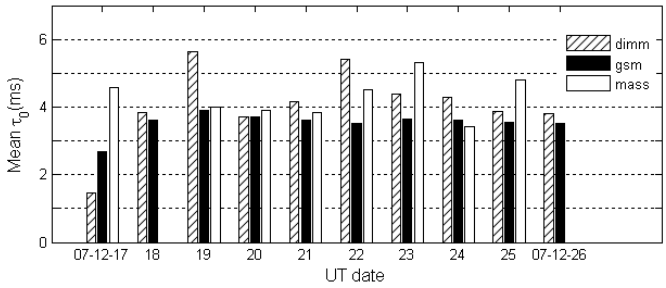

Fig. 7. Mean value of coherence time computed on all data delivered by ESO-DIMM, GSM, and MASS for ten nights at Paranal.

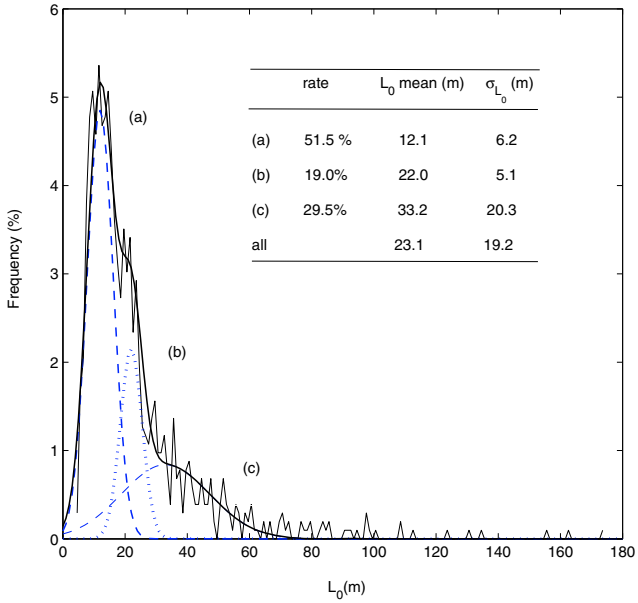

Fig. 8. Normalized histograms of outer scale measured with GSM, the curve with solid line shows the fit of the distribution by a sum of three log-normal functions. The separation of the three peaks is presented with three curves (a), (b), and (c) in dotted lines. The mean values, standard deviations, and fraction of each component are listed.

at which the structure function reaches the $\frac{1}{e}$ of this maximum corresponds to the GSM τ_{AA} (Ziad et al. 2004).

We plot in Fig. 6 the nightly value of the coherence time measured with ESO-DIMM, GSM, and MASS-DIMM with the time sampling of 10 mn for ESO-DIMM and 5 mn for MASS-DIMM and GSM. The mean value computed for all data of each instrument for each night is given in Fig. 7. We note a difference in the τ_0 mean values that can be explained by the use of different methods and definitions of this parameter. The mean value of the coherence time measured by the ESO-DIMM, 4.06 ms, agrees with 3.90 ms measured in 2000. For the GSM, the mean value of τ_{AA} is 3.54 ms, while for the MASS the mean τ_0 is 5.17 ms. Note here that the mean values of the coherence time in some nights, e.g. first night, stand quite different because the instruments did not observe exactly in the same periods of the night.

4.4. Outer scale measurements

For the first time at Paranal vertical profiles of the outer scale are provided by the dedicated instrument MOSP. The $\mathcal{L}_0$ estimation using GSM consists of the measurement of the normalized covariance of the AA fluctuations on two pupils separated by the baseline B. The adjustment of the normalized covariance curve to the precalculated theoretical covariance gives the $\mathcal{L}_0$ value.

The normalized histogram of $\mathcal{L}_0$ measured during the whole campaign is presented in Fig. 8. The histogram was fitted by a sum of three log-normal distributions (a), (b), and (c), plotted separately. For each of these components we give the mean value of $\mathcal{L}_0$ and its standard deviation. Therefore, we can suppose that each log-normal distribution corresponds to a specific turbulent regime (mode). The mode (a) corresponds to the case of small outer scale (~12 m), the mode (c) to the high value (~33 m) and (b) to the intermediate value (~22 m). Low values of $\mathcal{L}_0$ occur in 51% of the entire data set, 29.5% for high values and 19% for intermediate values.

We show in Fig. 9 the mean values of $\mathcal{L}_0(h)$ night by night as measured with MOSP, in addition to the mean values measured by the GSM. The value averaged over the whole campaign is 20.3 m for MOSP and 23.1 m for the GSM. This agrees with 20.0 m measured in 1998 at Paranal (Martin et al. 2000).

The outer scale $\mathcal{L}_0$ is a parameter of the Von Karman turbulence model. A combination of several turbulent layers with different $\mathcal{L}_0$ does not result in the Von Karman spectrum. For this reason, a definition of the integrated or equivalent $\mathcal{L}_0$ in the

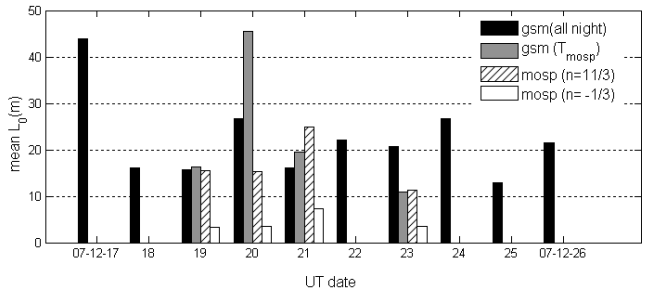

Fig. 9. Nightly outer scale mean value computed for all data delivered by GSM in dark bars and by MOSP in white bars. The outer scale computed in the overlapping time of GSM and MOSP is given as grey bars.

multi-layer case is ambiguous. A general formula was proposed by Maire et al. (2007):

$$\mathcal{L}_0^n = \frac{\sum \delta h_i C_n^2(h_i) \mathcal{L}_0^n(h_i)}{\sum \delta h_i C_n^2(h_i) \mathcal{L}_0(h_i)} \cdot \tag{9}$$

Borgnino (1990) found that for AA fluctuations $n = -1/3$ is appropriate. Here we find that the $n = 11/3$ exponent gives the best match between the GSM and MOSP outer scale values (Fig. 9), which agree with the suggestion of Maire (2007) and Maire et al. (2007).

5. Vertical distribution of turbulence at Paranal

In this section, we present both outer scale and energy profiles of turbulence at Paranal during the December 2007 campaign.

5.1. Outer scale profiles at Paranal

The profiles of $\mathcal{L}_0(h)$ determined with MOSP are shown in Fig. 10. As we can see, the outer scale values in the ground layer are typically a few meters (~10 m), the maximum value (~35 m) appears in the boundary layer at 1 km, after it decreases again to a few meters at around 3.5 km, above this layer it increases with height with an average value of ~20 m. If we compare this distribution, which shows three typical layers to the outer scale measured with GSM in Sect. 4.4, one can note an interesting coincidence with the three modes of the outer scale. Thus, we can suppose that each mode occurs when the turbulence in one of these three layers is dominating. Therefore, the low value of the outer scale given by the mode (a) in Fig. 8 can be related to the case where the turbulence in the ground layer is dominant, as was previously observed by Ziad et al. (2008) at Dome C.

5.2. Turbulence profiles at Paranal

The turbulence energy in each range of altitudes is described by the integral $\int C_n^2(h)\mathrm{d}h$ over this range.

First we sub-divide the total path (TOT) in only two zones, the ground layer (GL) below 500 m and the free atmosphere (FA) above 500 m. For this task, we consider all values of the total energy measured by the ESO-DIMM, GSM, and Cute-SCIDAR during the whole campaign in one block, and calculate the corresponding histograms. For the FA turbulence, we consider the values measured by the MASS and those given by the Cute-SCIDAR above 500 m. This increases the data count for a better statistics and also alleviates the difference in time-acquisition sampling between the instruments, if considered separately.

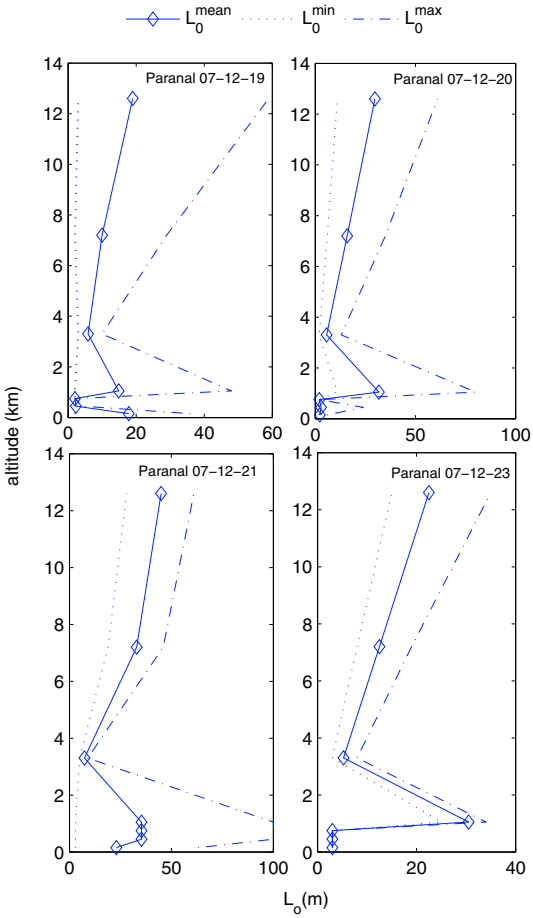

Fig. 10. Outer scale profiles measured with MOSP for four nights at Paranal, the mean value in solid lines, minimum value in dotted lines, and maximum value in dashed lines.

Once normalized, the histograms can be compared. We note from Fig. 11a that the energy distribution shows a log-normal behavior with two peaks, one at $5.49 \times 10^{-13}(m^{1/3})$, this corresponds to a seeing of 0.88 arc-sec, and the second peak at $1.95 \times 10^{-12}(m^{1/3})$ which corresponds to a seeing of 1.87 arc-sec. Despite the low probability (5.4%) to get this bad seeing value, it biases the mean value of the seeing, as we can see by comparing with the value given in Sect. 4.1.

The histogram of the FA energy is given in Fig. 11b. From each histogram we calculate average values of energy of the corresponding layer, which we show in Fig.11c. Thus, the difference between the average energy value of TOT and FA turbulence corresponds to the energy of the GL. Furthermore, the ratio GL/TOT and FA/TOT corresponds to the energy contribution of GL (respectively FA). Therefore, the contribution of FA is 28%. This means that 72% of the total energy is concentrated in the first 500 m above ground.

6. Surface layer identification

We focus here on the energy distribution below 500 m. We analyzed the LuSci data, which give $C_n^2(h)$ profiles at $h < 256$ m. We also estimated indirectly the turbulence energy by comparing the results of two independent instruments that are located at different heights – the ESO-DIMM and the GSM. In the following

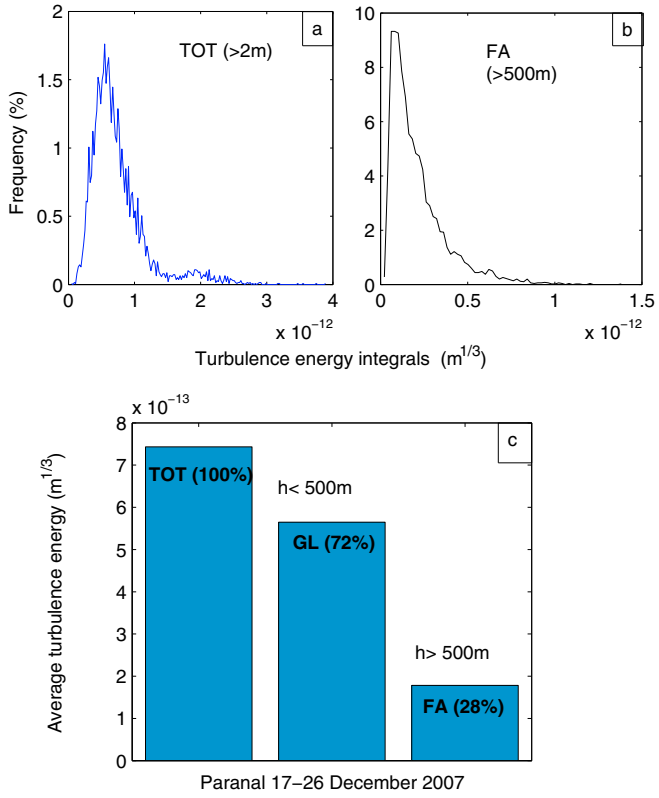

Fig. 11. **a)** normalized histogram of the total turbulence energy TOT integrated above ground; **b)** normalized histograms of the FA energy. The average energy for TOT and FA turbulence is calculated from the corresponding histograms and shown in **c)**. The energy of the ground layer GL is given by the difference between TOT and FA energies.

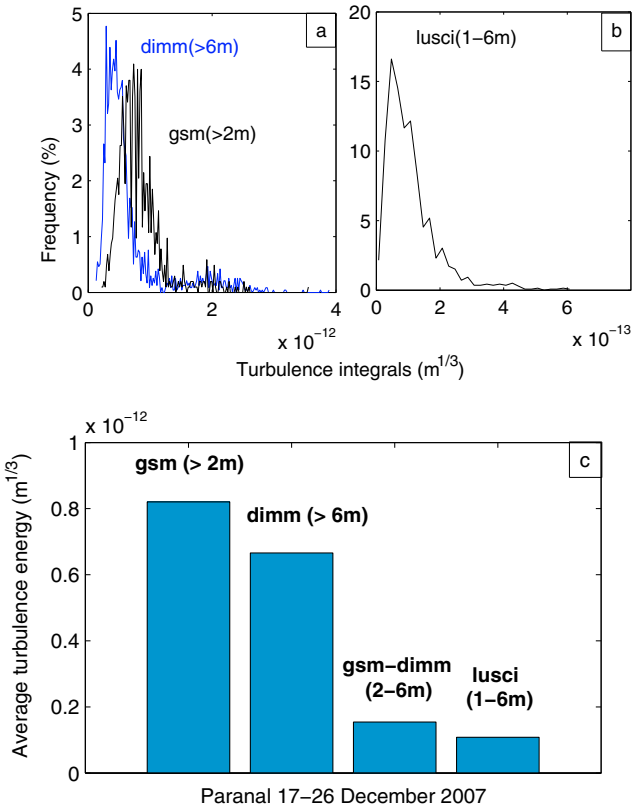

Fig. 12. **a)** Normalized histograms of the total turbulence energy TOT integrated from 2 m above ground by GSM and above 6 m with DIMM. **b)** shows the energy of 1 to 6 m layer given by LuSci and the corresponding average energy in figure **c)**, we also compare the difference of the total energy between DIMM and GSM and the energy of the same layer measured by LuSci.

we assume that these site monitors do not introduce additional turbulence themselves, which may be not quite true.

In this campaign, we had the advantage of setting LuSci and GSM near the ESO-DIMM tower. This allowed us to compare the energy integrated from 2 m upward with GSM and from 6 m up with ESO-DIMM. The returned histograms are shown in Fig. 12a. We compare this with the energy integrated from 1–6 m measured by LuSci (Fig. 12b). The difference of the average values of energy between GSM and ESO-DIMM given in Fig. 12c is similar to the value measured by LuSci. This confirms that the difference between ESO-DIMM and GSM is caused by turbulence located below 6 m; this layer alone contributes 18% to the total energy.

From Figs. 11a,b and 12a,b we note that the histograms present three distinct distributions as in case of the outer scale given in Sect. 4.4. One can assume that this is due to the SL, as was noted at Dome C by Aristidi et al. (2009). Their study was built on a longtime series of measurements during several years and for a complete night's covering. The data collected during the ten nights of our campaign did not allow us to reach the same conclusion about the seeing regimes.

We can evaluate the mean turbulence profile $C_n^2(h)$ at Paranal during this campaign by combining the results from five independents instruments (Table 1). We then obtain good altitudes sampling including the GL and FA, as well as the SL turbulence.

In Fig. 13 we show the reconstructed mean profile of $C_n^2(h)$. Let us compare it to the existing models. We note a good agreement with the Hufnagel-Valley model, except for the first 100 m above ground, where $C_n^2(h)$ exhibits a power-law dependence on height as $h^{-0.85}$. The power law dependence of $C_n^2(h)$ on height was noted in the previous campaigns at Paranal with $h^{-0.87}$ in 1998 (Martin et al. 2000). Recently Chun et al. (2009) proposed an exponential dependence of turbulence on height in the surface layer at the Mauna Kea site.

Assuming that $C_n^2(h) \propto h^{-0.85}$, the turbulence integral in the SL (from $h = 0$) becomes proportional to $h^{-0.85+1}$. For example, 80% of the energy in the first 100 m is concentrated below 25 m because $(25/100)^{0.15} = 0.8$. The power-law profile does not allow for any reasonable definition of the SL thickness or upper boundary.

Table 1. Mean value of $C_n^2(h)$ at different altitudes for the December 2007 campaign at Paranal.

h(m)	$\log_{10} C_n^2(h)$	h(m)	$\log_{10} C_n^2(h)$
1.5	–13.68	3000	–16.89
3.0	–13.74	5000	–17.23
4.5	–13.82	6000	–17.37
16	–14.84	7000	–16.86
64	–14.83	8000	–16.96
128	–15.05	12 000	–17.22
143	–15.39	12 500	–16.66
250	–15.04	15 000	–16.94
700	–15.88	20 000	–18.75
2000	–16.43	25 000	–18.40

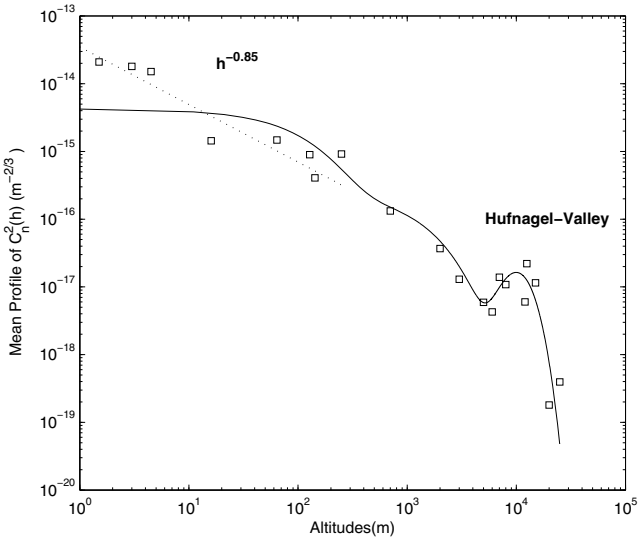

Fig. 13. Reconstructed $C_n^2(h)$ mean profile at Paranal for the December 2007 campaign using the simultaneous measurements of the energy at different altitudes and different height sampling plotted in squares. We show the Hufnagel-Valley model in solid line and the adjustment of the first meters layer to a power law of height $h^{-0.85}$ in dotted lines.

In consequence, the SL turbulence strongly affects the ATs and the UTs much less because of their 30 m high enclosures. Nevertheless, there might be an indirect effect owing to the interaction between these enclosures and the SL. This occurs when the wind screens and louvers are opened during observations, particularly when observing far from the zenith. This exposes the primary mirror to a part of the surface layer.

7. Conclusion

Statistics of optical turbulence parameters – seeing, isoplanatic angle, coherence time, and the outer scale of wavefront – are presented in this paper. We compared our results with the previous campaigns at Paranal and found a good agreement.

For the first time, we were able to measure the profiles of the outer scale at Paranal. They show a low value for the ground layer. We could not measure the outer scale near the ground; it will be interesting to do this in the future.

By comparing the statistical results of the outer scale measured by GSM and the profiles given by MOSP, we identified three typical values of the outer scale and related them to the dominating turbulence in the ground layer, in the boundary layer (1 km), and above 3.5 km.

Finally, the statistical analysis of the energy profiles reveals a significant contribution of the surface layer to the seeing degradation. The mean profile of the turbulence energy given in this paper is representative of only the period of this campaign. It will be very useful to see the seasonal and annual characteristic of the turbulence profile at Paranal by making a long series of measurement.

Acknowledgements. This work has been funded by European Community under contract number 011863 ELT Design Study with the participation of ESO, IAC, OCA reported under reference ELT-TRE-UNI-12300-0001. We are grateful to CTIO for the loan of LuSci and the related data reduction support.

References

Aristidi, E., Fossat, E., Agabi, A., et al. 2009, A&A, 499, 955
Avila, R., Vernin, J., & Masciadri, E. 1997 Appl. Opt., 36, 7898
Borgnino, J. 1990, Appl. Opt., 29, 1863
Chun, M., Wilson, R., Avila, R., et al. 2009, MNRAS, 394, 1121
Dali Ali, W., Ziad, A., Berdja, A., et al. 2009 Proc. OTAM (Imperial College Press), 108
Fried, D. L. 1976, SPIE, 20, 7898
Kornilov, V. G., Tokovinin, A., Vozyakova, O., et al. 2003, SPIE, 4839, 837
Maire, J., Borgnino, J., Mourard, D., et al. 2006, A&A, 448, 1225
Maire, J. 2007, Ph.D Thesis University of Nice Sophia-Antipolis
Maire, J., Ziad, A., Borgnino J. & Martin, F. 2007, MNRAS, 377, 1236
Maire, J., Ziad, A., Borgnino, J., & Martin, F. 2008, MNRAS, 386, 1064
Martin, F., Conan, R., Tokovinin, A., et al. 2000, A&AS, 144, 39
Rajagopal, J., Tokovinin, A., Bustos, E., & Sebag, J. 2008, SPIE, 7013, 60
Roddier, F. 1981, Progr. Opt., 19, 281
Roddier, F., Gilli, J. M., & Vernin, J. 1982, J. Opt., 13, 63
Sarazin, M. 1986, SPIE, 628, 138
Sarazin, M., & Roddier, F. 1990, A&A, 227, 294
Sarazin, M., & Tokovinin, A. 2002, ESO Conf., 58, 321
Tokovinin, A. 2007, Rev. Mex. Astron. Astrofis., 31, 61
Tokovinin, A., & Kornilov, V. 2007, MNRAS, 1, 13
Tokovinin, A., Bustos, E., & Berdja, A. 2010, MNRAS, 404, 1186
Vazquez Ramio, H., Delgado, J. M., Reyes, M., et al. 2008, SPIE, 7012, 45
Ziad, A., Conan, R., Tokovinin, A., et al. 2000, Appl. Opt., 39, 5415
Ziad, A., Schöck, M., Chanan, G. A., et al. 2004, Appl. Opt., 43, 2316
Ziad, A., Aristidi, E., Agabi, A., et al. 2008, A&A, 491, 917